

# Micro-motion Forms Classification of Space Cone-shaped Target Based on Convolution Neural Network

Gaogui Xu<sup>1,2</sup>, Hongcheng Yin<sup>1,2</sup>, and Chunzhu Dong<sup>2</sup>

<sup>1</sup> School of Information Engineering  
Communication University of China, Beijing 100024, China  
edward2016@cuc.edu.cn

<sup>2</sup> Science and Technology on Electromagnetic Scattering Laboratory  
Beijing 100854, China

**Abstract** — In this paper, the echo models with different micro-motion forms (spin, tumbling, precession, and nutation) of space cone-shaped target are built. Different from the ideal point scatterers model, the radar echo contains the contribution from the complex radar cross section (RCS) of point scatterer vs aspect angle. And a convolution neural network (CNN) model for micro-motion forms classification based on the micro-Doppler characteristics in spectrograms is presented. The simulation results show that our method can discriminate different micro-motion forms effectively and the overall accuracy is 97.24%. Different levels of additive white Gaussian noise are added to simulate noise-contaminated radar echo. It has been found that the presented method has a stronger anti-noise ability than support vector machine (SVM). When the Signal-to-Noise Ratio (SNR) of Gaussian white noise is 10 dB, the overall accuracy of our algorithm is 29.79% higher than that of SVM.

**Index Terms** — Convolution neural network, micro-Doppler, micro-motion forms classification, space cone-shaped target.

## I. INTRODUCTION

The micro-Doppler effect refers to Doppler modulations on the radar echo due to micro-motion dynamics (such as mechanical vibrations or rotations) of the target or any structure on the target, in addition to the constant Doppler frequency shift induced by the bulk motion of a radar target [1, 2]. Micro-Doppler is a unique signature of the target with movements and provides additional target features that are complementary to existing methods [2]. The micro-Doppler effect can be used to classify and identify the target, for example, human detection and activity classification [3] and the warhead and decoys of ballistic target [4].

Due to the interference by releasing decoys and the wobble under the action of the Earth's atmosphere,

besides the translation along the line of sight (LOS) of the radar, the warhead will have spin, precession, and nutation. Many researches indicated that the micro-Doppler signatures can be used to recognize and discriminate the warhead and the decoys [4-6]. The micro-motion parameters of the ballistic target reflect the important characteristics such as its structure, size, and micro-motion period. For radar imaging, to obtain a clear body image, the micro-Doppler component must be separated [7-9]. The premise of the success of these methods is to extract stable and effective micro-motion signatures.

Conventionally, the micro-motion parameters estimation methods are based on the micro-motion form [10, 11]. However, it's hard to know the micro-motion form of the target, since radar usually observes non-cooperative targets. And the traditional classification methods of micro-motion forms can be regarded as a kind of feature engineering, which means that they need to extract discriminative features from the raw echo data for classification algorithms.

In general, the domain knowledge of micro-Doppler signals is required either in the design of time-varying signatures or from the extraction of features. These limitations result in poor adaptability of the algorithm and low anti-noise capability. In this paper, we propose a deep convolution neural network (CNN) model, which is based on the classical CNN devised by LeCun *et al* [12]. It can effectively discriminate the micro-motion forms from the radar echo, which makes the application of the parameter estimation methods more successful. CNN is an end-to-end learning that automatically learns features and discriminates patterns from data. Compared with the traditional method, CNN takes feature design, feature selection, feature extraction, and pattern recognition as a whole by optimizing a certain loss function. Through automatic learning features, it has achieved state-of-the-art results in many fields, such as

image classification [13, 14] and speech recognition [15, 16]. Thus, the influence of the preorder algorithm module on the subsequent algorithm module is reduced.

This paper is organized as follows: in Section II, we develop the echo models of space cone-shaped target with four different micro-motion forms, and the details of the classification algorithm based on CNN are described. Next, in Section III, the simulation results are given, followed by the conclusion in Section IV.

## II. MICRO-MOTION FORMS CLASSIFICATION

### A. Mathematical model

With the development of modern penetration technology, cone-shaped decoys have appeared. Since the attitude control of the decoy is weak, the angle of precession and nutation will be larger, and even the decoy will tumble. Therefore, the echo models of four different forms of micro-motion (spin, tumbling, precession, and nutation) are given.

Figure 1 gives the geometry of radar and cone-shaped target with spin, tumbling, precession, and nutation. Three coordinate systems are introduced. The radar is stationary and located at the origin of the radar coordinate system  $(U, V, W)$ . The cone-shaped target is located at the local coordinate system  $(x, y, z)$  and spinning around its symmetric axis  $\vec{O}'z$ . The origin of the local coordinate system is at the center of mass of the target. The reference coordinate system  $(u, v, w)$  is parallel to the radar coordinate system and shares the origin with the local coordinate system. The origin  $O'$  is assumed to be at a distance  $R_0$  from the radar.

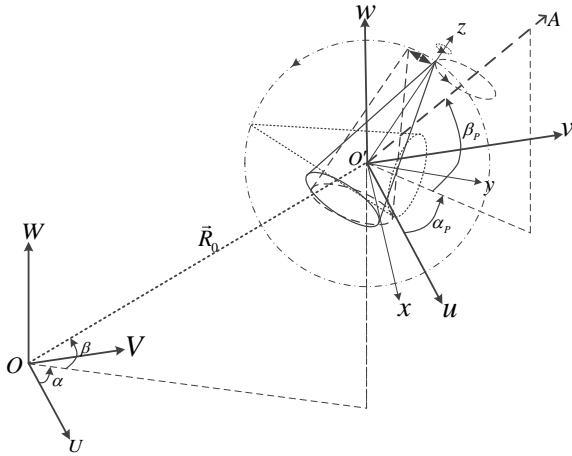


Fig. 1. Geometry of radar and cone-shaped target with spin, tumbling, precession, and nutation.

For simplicity, a target can be represented as a set of point scatterers. In the interest of brevity, the scatterer in the following text refers to the point scatterer. Under

high-frequency electromagnetic waves, the scatterers of a cone-shaped target are mainly composed of cone top  $P_0$  and two cone bottoms  $P_1$  and  $P_2$ . If the radar transmits a sinusoidal waveform with a carrier frequency  $f_0$ , then the baseband of the returned signal from the cone-shaped target is:

$$s(t) = \sum_{i=0}^2 \sqrt{\sigma_i} \exp\{j\varphi_i\} \exp\left\{j2\pi f_0 \frac{2R_i}{c}\right\} \quad (1)$$

$$= \sum_{i=0}^2 RCS_i \exp\left\{j2\pi f_0 \frac{2R_i}{c}\right\},$$

where  $c$  is the speed of the electromagnetic wave propagation,  $R_i$  is the range from the radar to the scatterer  $P_i$ , and  $RCS_i = \sqrt{\sigma_i} \exp\{j\varphi_i\}$  is the complex radar cross section (RCS) of the scatterer  $P_i$ , which will vary in different attitudes, as shown in the Appendix.

It is worth noting that the location of the scatterer  $P_i (i = 0, 1, 2)$  is not fixed, and it will slide on the surface of the target. For example, scatterer  $P_0$  is a moving scatterer that slides on the surface of the spherical crown with the change of incident direction. The location of  $P_0$  is the point at which the incident ray passes through the center of the sphere and intersects with the sphere.

Suppose a scatterer  $P$  is located at  $\vec{r}_0 = (x_0, y_0, z_0)^T$  represented in the target local coordinate system  $(x, y, z)$  at instant of time  $t = 0$ , where the superscript  $T$  means transposition. Generally, the local coordinate system and the reference coordinate system do not coincide at the initial time. For the reference coordinate system, the position of point  $P$  at time  $t = 0$  can be calculated as  $R_{init} \cdot \vec{r}_0$ , where  $R_{init}$  is an initial rotation matrix determined by Euler angles. After rotation, the point  $P$  in the radar coordinate system at time  $t = 0$  is located at  $\vec{R}_0 + R_{init} \cdot \vec{r}_0$ .

Since the space cone-shaped target is rotationally symmetrical, its spin does not affect radar echo. Thus, the echo is obtained as:

$$s_1(t) = \sum_p RCS_p \exp\left(j \frac{4\pi}{\lambda_0} \left\| \vec{R}_0 + R_{init} \cdot \vec{r}_0 \right\| \right), \quad (2)$$

where  $\lambda_0$  is the wavelength and  $\|\cdot\|$  represents the Euclidean norm.

In the process of unfolding, the force of decoy is more complex, which will cause its tumbling motion to be irregular. For simplicity, suppose that the target will tumble around the center of mass about its axes  $x, y, z$  with an angular velocity  $\vec{\omega} = (\omega_x, \omega_y, \omega_z)^T$ . Therefore, the unit vector of  $\vec{\omega}$  is  $\vec{\omega}' = (\omega'_x, \omega'_y, \omega'_z)^T = \vec{\omega} / \|\vec{\omega}\|$ . According to Rodrigues formula [17], at time  $t$  the rotation matrix becomes:

$$R_t = I + \hat{\omega}' \sin \Omega t + \hat{\omega}'^2 (1 - \cos \Omega t), \quad (3)$$

where  $\Omega = \|\vec{\omega}\|$ ,  $\hat{\omega}'$  is a skew symmetric matrix constructed by  $\vec{\omega}'$ .

After tumbling, the echo can be expressed as:

$$s_2(t) = \sum_P RCS_P \exp\left(j \frac{4\pi}{\lambda_0} \left\| \left( \vec{R}_0 + R_t \cdot R_{init} \cdot \vec{r}_0 \right) \right\| \right). \quad (4)$$

Precession refers to the coning motion of a target along the axis  $\vec{O'A}$ , in addition to spinning around its symmetry axis  $\vec{O'z}$ , as shown in Fig. 1. The angle between axis  $\vec{O'A}$  and axis  $\vec{O'z}$  is called the precession angle. Spinning and coning are both rotating motions, except that the axis of rotation is different. Therefore, Precession can be regarded as the spin of the target in the local coordinate system and then the coning motion in the reference coordinate system. At time  $t$ , the location of the scatterer  $P$  in the reference coordinate system is  $R_c \cdot R_{init} \cdot R_s \cdot \vec{r}_0$ , where  $R_c$  is the rotation matrix of coning motion and  $R_s$  is the rotation matrix of spinning motion, both of which are determined by equation (3). Thus, the echo of micro-Doppler modulations induced by precession is:

$$s_3(t) = \sum_P RCS_P \exp\left(j \frac{4\pi}{\lambda_0} \left\| \left( \vec{R}_0 + R_c \cdot R_{init} \cdot R_s \cdot \vec{r}_0 \right) \right\| \right). \quad (5)$$

If the precession angle does not remain at a constant, the target will oscillate up and down between two limits. This motion is called nutation. After precession, the transient position vector of symmetry axis  $\vec{O'z}$  is  $\vec{z}_t = R_c \cdot R_{init} \cdot [0,0,1]^T$ . The target will then oscillates in the plane composed of vector  $\vec{z}_t$  and unit vector  $\hat{x} = \vec{O'A}$ . It is equivalent to rotating about the axis  $\hat{z} = \vec{O'A} \times \vec{z}_t$ , where  $\times$  represents cross multiplication.

Therefore,  $x' = \hat{x}$ ,  $y' = \hat{z} \times \hat{x} / \|\hat{z} \times \hat{x}\|$ , and  $z' = \hat{z} / \|\hat{z}\|$  form a new coordinate system. The transition matrix from the reference coordinate system  $(X, Y, Z)$  to the new coordinate system is  $A = (x', y', z')$ . The rotation matrix of the target rotating around the  $z'$  axis is  $B$ , which is determined by oscillating frequency  $f_o$  and oscillating amplitude  $\theta_o$ . Then, the echo is obtained as [2]:

$$s_4(t) = \sum_P RCS_P \exp\left(j \frac{4\pi}{\lambda_0} \left\| \left( \vec{R}_0 + R_v \cdot R_c \cdot R_{init} \cdot R_s \cdot \vec{r}_0 \right) \right\| \right), \quad (6)$$

where  $R_v = A \cdot B \cdot A^T$ .

## B. Micro-motion forms classification based on convolution neural network

As shown in equations (2), (4), (5), and (6), the echoes of the target with different micro-motion forms are very different. In frequency domain, the common method for analyzing echo signal is Fourier transform. Due to lack of localized time information, it is not suitable for analyzing a signal whose frequency changes over time. Compared with Fourier transform, a joint time-frequency analysis can provide localized time-dependent frequency information, which is used to

extract time-varying signatures for micro-motion forms classification. In this paper, the Wigner-Ville distribution (WVD) [18] is used to analyze the micro-Doppler.

Different micro-motion forms present their unique micro-Doppler signatures. The micro-Doppler modulation caused by different micro-motion forms can be seen in the high-resolution spectrogram. By using spectrograms, we convert the micro-motion forms classification problem to an image recognition problem. Figure 2 shows the hierarchical structure of the CNN, which stacks multiple layers of simple neural network architecture, thus extracting the representation of data layer by layer. It takes color spectrograms as the input and learns the mapping between the spectrogram and its corresponding micro-motion form. CNN is mainly composed of four components. The first component is the convolution layer which consists of a set of learnable filters. Each filter has small receptive fields of input data and can be seen as a specific feature extractor. However, in convolution operation, if there is no nonlinear transformation in the network, the network will only learn the linear characteristics of the input, resulting in the network can't deal with nonlinear problems, and the application scene is limited. The second component is the nonlinear activation function that carries on the nonlinear transformation to the result of the linear transformation. The commonly used activation functions are the Sigmoid function, the Restricted Linear Units (ReLU) function, and their variants. In this paper, we choose ReLU as the activation function, the formula of which is  $f(x) = \max(0, x)$ . The third component is the pooling layer, which subsamples the data according to certain rules while retaining the main information. By performing  $2 \times 2$  pooling operation with max pooling, the data size will be halved. Thus, The pooling layer greatly reduces the network parameters and prevents overfitting.

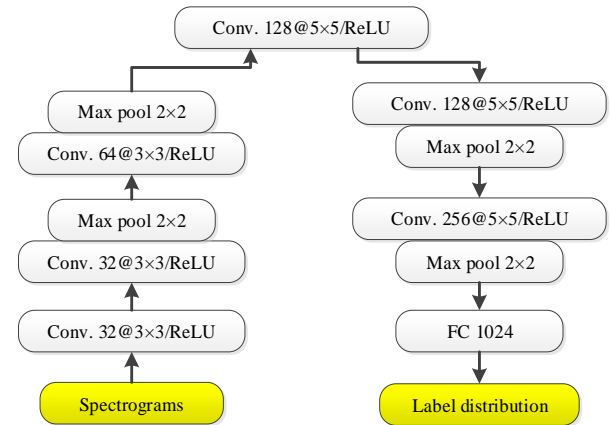


Fig. 2. The hierarchical structure of the CNN.

The last component is the full connection layer

(FCN), where all the input nodes are connected to all the output nodes. In the classification problem, Softmax function is typically used as an activation function for the output layer to obtain the probability of the category and can be expressed as:

$$a_i = e^{z_i} / \sum_{j=1}^L e^{z_j}, \quad (7)$$

where  $L$  represents the total number of target categories.

The category of the target is determined by the neuron with the highest probability, which is  $\text{argmax}(a)$ .

Suppose the difference between the network output and the real value is  $\text{loss}(x)$ , which is called the error function. The training of CNN can be divided into two processes: forward propagation and backward propagation. In the forward propagation, the output of the network is calculated according to the input image. And in the backward propagation, the network parameters are automatically updated by the error function. This parameter update method is called gradient descent (GD). It is an optimization method to find a local (preferably global) minimum of a function. For the network parameter  $w_{ij}$ , it is updated using:

$$w_{ij}^{\tau+1} = w_{ij}^{\tau} + \Delta w_{ij}^{\tau}, \quad (8)$$

where  $\tau$  is the gradient descent iteration and  $\Delta w_{ij}^{\tau}$  is the weight update.

$\Delta w_{ij}^{\tau}$  is determined by:

$$\Delta w_{ij}^{\tau} = -\eta \frac{\partial \text{loss}(x)}{\partial w_{ij}}, \quad (9)$$

where  $\eta$  is the learning rate and  $x$  is the input spectrogram.

According to the number of input samples used for each update of the weights, two variants of GD are generally used, namely on-line learning and batch learning. In on-line learning, the weights are updated for every input. In batch learning, the error function is calculated for a batch of input samples. If the selection of the input samples is random, the GD optimization method is called stochastic gradient descent (SGD). In this paper, the SGD is used and the batch size is 256.

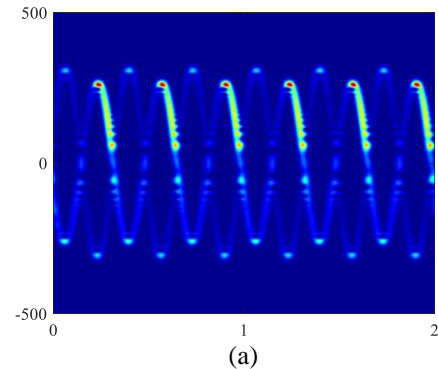
### III. SIMULATION RESULT

The echoes of four micro-motion forms are simulated and WVD is used to obtain the spectrograms. Assume that the operating frequency of radar is 10 GHz and the center of mass of the target is located at ( $U = 1000m, V = 5000m, W = 5000m$ ). The azimuth angle  $\alpha_p$  and elevation angle  $\beta_p$  of the coning axis  $\vec{O'A}$  range from  $10^\circ$  to  $80^\circ$  with an interval of  $5^\circ$ . Thus, there are 225 combinations of  $(\alpha_p, \beta_p)$  pairs. The initial Euler angles are  $(30^\circ, 30^\circ, 45^\circ)$ . For spin, the spinning frequency is from 1 Hz to 20 Hz with an interval of 0.5 Hz. Assume that the range of each component of the angular velocity of rotation  $\vec{\omega}$  is from  $\pi/2$  rad/s to

$8\pi$  rad/s with an interval of  $\pi/4$ . Compared with spin, precession has rotation around the coning axis, and the frequency of rotation is from 2 Hz to 5 Hz with an interval of 0.5 Hz. Nutation is a periodic transformation of the precession angle based on precession. Assume that the wobble frequency is from 5 Hz to 7 Hz with an interval of 0.5 Hz and that the oscillating amplitude ranges from  $1^\circ$  to  $5^\circ$  with an interval of  $1^\circ$ .

Suppose that the radar pulse repetition frequency (PRF) is 2000. The spectrograms are obtained by WVD analysis of 2s echo data. Since the RCS is related to polarization, the horizontal to horizontal (HH) and vertical to vertical (VV) polarization are considered. If the simulation is carried out according to the above conditions, the samples of each micro-motion form are uneven. Combined with the limited information contained in the spin, for precession, we randomly select 21 frequencies from the spin frequencies, resulting in 66,150 data. For nutation, we randomly select one frequency from the spin frequencies, resulting in 78,750 data. The size of the spectrogram is normalized to  $256 \times 256$ .

In order to further approach the actual case, we consider not only the contribution from the complex RCS of point scatterer vs aspect angle, but also the change of the scatterer's location with target motion. They will have an impact on micro-Doppler modulation, making it difficult for the feature-based classification algorithms to discriminate different micro-motion forms. Figure 3 shows an example of spectrograms of a cone-shaped target with precession for HH and VV polarization. There are two visible scatterers in the time of 2 seconds, as shown in Fig. 3 (a). The curves of scatterer  $P_0$  and scatterer  $P_1$  are sinusoidal curve. The RCS of scatterer  $P_1$  is smaller for VV polarization than for HH polarization, resulting in discontinuity of its curve, as shown in Fig. 3 (b). Different polarization only affects the continuity of the curve and does not change the micro-Doppler characteristics of the target. Among the 176,400 data, 80% of spectrograms of each micro-motion form are used as the training set and the rest as the test set. The convolution neural network shown in Fig. 2 is constructed.



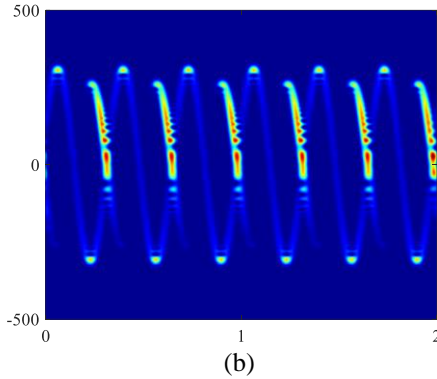


Fig. 3. Micro-Doppler modulations of cone-shaped target induced by precession for (a) HH and (b) VV polarization.

Different micro-motion parameters, such as the rotation frequency, will have effect on the amplitude and the period of the curve in spectrograms. The distinctions of different micro-motion forms are the curve characteristics of scatterers. The rotationally symmetrical target with spin does not effect micro-Doppler modulation. The micro-Doppler frequency shift is approximately 0. Thus, there is not much information contained in spectrogram, which is often a widened straight line. As far as tumbling is concerned, the amplitudes of different scatterers are the same. The difference between precession and tumbling is the amplitude of the curves. Although they are both sinusoidal curves, for precession, the amplitudes of curves are different. For nutation, there will be no more sinusoidal curves. The micro-Doppler of scatterers is modulated by the mixing of spinning, coning, and oscillating. At the same time, different polarizations will affect the continuity of the curve. Therefore, the method based on feature engineering is difficult to extract effective curve features from spectrograms, especially under noise. Different from other feature based classification algorithms, CNN learns from a large

number of spectrograms to extract the common features in the same class and ignore the differences. It automatically extracts the features related to the classification tasks, so as to achieve higher accuracy than the traditional algorithm.

With the increase of training epochs, the error on the training set becomes smaller and smaller, while the error on the test set decreases first and then increases. At this time, the network is overfitted. After 200 epochs, the parameters of the network are approximately optimal, and the overall accuracy is 97.24%. The confusion matrix for the micro-motion forms classification based on CNN is listed in Table 1. Each column in the table is the predicted label, each row is the true label, and the diagonal element is the number correctly classified. The last column is the classification accuracy of each category. In order to measure the overall performance of the algorithm in multiple classification problems, the overall accuracy is introduced, which can be expressed as:

$$OA = \frac{1}{N} \sum_{i=1}^n C_{ii}, \quad (10)$$

where  $N$  is the number of total samples,  $n$  is the number of categories, and  $C_{ii}$  is the number correctly classified for class  $i$ .

For spinning and tumbling, due to their simple micro-motion, their classification accuracy is higher. When the oscillating amplitude of the target is small or the wobble frequency is slow, the difference between nutation and precession will become smaller, and it is easy to misjudge the nutation as precession. However, the classification accuracy of nutation is still above 95%. In contrast, the support vector machine (SVM) which is a feature-based classification algorithm is also used for micro-motion forms classification. Since the size of spectrograms is  $256 \times 256$ , the number of features is too large for SVM. Therefore, we use the principal component analysis (PCA) as a pre-processing. The overall accuracy of SVM is 72.69%. It is 24.55% lower than that of CNN, which is identical to the theoretical analysis.

Table 1: Confusion matrix for the micro-motion forms classification based on CNN

	Spin	Tumbling	Precession	Nutation	Accuracy (%)
Spin	3510	0	0	0	100
Tumbling	0	2715	63	12	97.31
Precession	0	59	12704	467	96.02
Nutation	0	139	548	15063	95.64

Additive Gaussian white noise of various Signal-to-Noise Ratio (SNR) levels (5, 10, 15, and 20 dB) are added to simulate noise-contaminated radar echoes. Figure 4 demonstrates the anti-noise capability of the two algorithms. With decreasing SNR, the performance of these algorithms decreases. The key point used to distinguish precession from nutation is that the micro-Doppler

modulation of scatterer  $P_0$  is a sinusoidal curve. The sinusoidal curve will be destroyed in a low SNR, thus the classification error will be increased. But it is clearly seen that the performance of our algorithm is very good. When the SNR is 10 dB, the overall accuracy of our algorithm is still 91.03%, which is 29.79% higher than that of SVM. Therefore, our method has strong anti-noise capability.

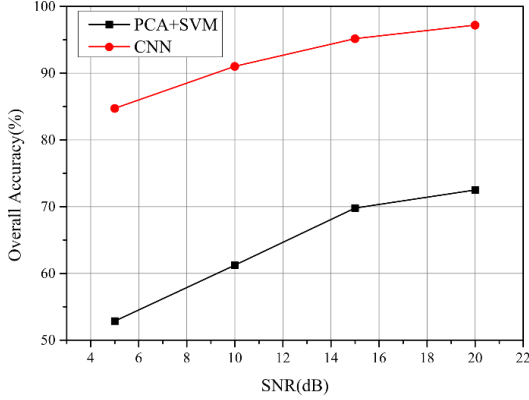


Fig. 4. The anti-noise capability with Gaussian noise.

#### IV. CONCLUSION

In this paper, we describe the complex RCS variation in the target's different attitudes; develop the echo models of space cone-shaped target with different micro-motion forms (spin, tumbling, precession, and nutation); propose a CNN model for micro-motion forms classification based on spectrograms. Compared with SVM, the method avoids artificial feature selection and feature extraction. Simulated results illustrate that CNN can exploit micro-Doppler features of space cone-shaped target and effectively discriminate different micro-motion forms. Since precession is a special kind of nutation with the oscillating amplitude  $\theta_n = 0$ , the overall accuracy of them has decreased somewhat. However, compared with SVM, ours has a higher overall accuracy. As a result, we found that our algorithm effectively suppresses noise. When the SNR is higher than 10 dB, the overall accuracy of our algorithm is higher than 90%.

#### APPENDIX

The sharp cone is a special case of the blunt cone, at which the radius of the spherical crown of the blunt cone is 0. Suppose the bottom radius of the blunt cone is  $a$ , the half cone angle is  $\alpha$ , and the spherical crown radius is  $b$ , as shown in Fig. 5.

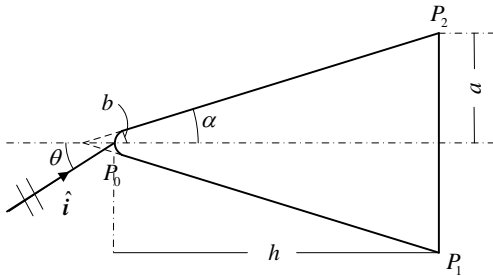


Fig. 5. Geometry of blunt-cone target.

The three scatterers are spherical crown  $P_0$  and two scatterers  $P_1, P_2$  on the bottom edge (the intersections of the incident surface and the bottom edge). Since the blunt cone is axisymmetric, its attitudes can be characterized by the included angle  $\theta$  between the incident ray and the symmetry axis of cone. Here,  $\theta$  ranges from 0 to  $\pi$ . For scatterer  $P_0$ , it is only visible in  $0 \leq \theta < \pi/2 - \alpha$ . Thus, the complex RCS of  $P_0$  is [19]:

$$\sqrt{\sigma_0} = \begin{cases} \pi^{\frac{1}{2}} b \left( 1 - \frac{\sin(2k_0 b (1 - \sin \alpha))}{k_0 b \cos^2 \alpha} \right)^{\frac{1}{2}}, & \theta = 0 \\ \pi^{\frac{1}{2}} b, & 0 < \theta < \frac{\pi}{2} - \alpha \\ 0, & \theta \geq \frac{\pi}{2} - \alpha \end{cases} \quad (11)$$

$$\varphi_0 = 0,$$

where  $k_0 = 2\pi/\lambda_0$ .

For scatterer  $P_1$ , its RCS is not only related to  $\theta$ , but also affected by polarization, which can be described as:

$$\sqrt{\sigma_1} = \frac{\sin \frac{\pi}{n}}{n} \sqrt{\frac{a}{k_0 \sin \theta}} \left( \left( \cos \frac{\pi}{n} - 1 \right)^{-1} \mp \left( \cos \frac{\pi}{n} - \cos \frac{3\pi - 2\theta}{n} \right)^{-1} \right) \quad (12)$$

$$\varphi_1 = \frac{\pi}{4}.$$

Here  $n = 3/2 + \alpha/\pi$ . The upper sign applies when the polarization is VV polarization while the lower sign applies if it is HH polarization.

When the electromagnetic wave is incident perpendicular to the conical surface, the divisor of equation (12) is 0. The RCS of scatterer  $P_1$  is mainly caused by the specular reflection of the conical surface.  $\sqrt{\sigma_1}$  should be calculated by the physical optical method [20, 21] and the maximum value is reached. At this point,  $\theta$  is equal to  $\pi/2 - \alpha$ , and the equation (12) can be modified to:

$$\sqrt{\sigma_1} = \left\{ \frac{4}{9} k_0 \frac{\cos^3 \alpha}{\sin^2 \alpha} \left[ a^{\frac{3}{2}} - (b \cos \alpha)^{\frac{3}{2}} \right]^2 \right\}^{\frac{1}{2}}. \quad (13)$$

Near  $\pi/2 - \alpha$ , if  $\sqrt{\sigma_1}$  calculated by equation (12) is greater than the maximum, it should be smoothed.

Unlike scatterer  $P_1$ , scatterer  $P_2$  is visible only when  $0 < \theta \leq \alpha$  or  $\theta \geq \pi/2$ . Its RCS is:

$$\sqrt{\sigma_2} = \begin{cases} \frac{\sin(\pi/n)}{n} \sqrt{\frac{a}{k_0 \sin \theta}} \left( \left( \cos \frac{\pi}{n} - 1 \right)^{-1} \mp \left( \cos \frac{\pi}{n} - \cos \frac{3\pi + 2\theta}{n} \right)^{-1} \right), & 0 < \theta \leq \alpha \\ 0, & \alpha < \theta < \frac{\pi}{2} \\ \frac{\sin(\pi/n)}{n} \sqrt{\frac{a}{k_0 \sin \theta}} \left( \left( \cos \frac{\pi}{n} - 1 \right)^{-1} \mp \left( \cos \frac{\pi}{n} - \cos \frac{\pi - 2\theta}{n} \right)^{-1} \right) & \theta \geq \frac{\pi}{2} \end{cases} \quad (14)$$

$$\varphi_2 = -\frac{\pi}{4}$$

The equations (12) and (14) give the variation of the RCS of the bottom scatterers  $P_1$  and  $P_2$  with different attitudes. When  $\theta$  is approximately 0 or  $\pi$ ,  $\sin \theta$  will approach zero, at which point the equations (12) and (14)

will become meaningless and need to be modified. When  $0 \leq \theta \leq \alpha$ , the contribution from scatterers  $P_1$  and  $P_2$  can be expressed as :

$$\sqrt{\sigma_1} e^{j\psi_1} + \sqrt{\sigma_2} e^{j\psi_2} = \frac{2\sqrt{\pi} a \sin \frac{\pi}{n}}{n} \left( \left( \cos \frac{\pi}{n} - \cos \frac{3\pi}{n} \right)^{-1} J_0(2k_0 a \sin \theta) - \frac{j \frac{2 \tan \theta}{n} \sin \frac{3\pi}{n}}{\left( \cos \frac{\pi}{n} - \cos \frac{3\pi}{n} \right)^2} J_1(2k_0 a \sin \theta) \mp \left( \cos \frac{\pi}{n} - 1 \right)^{-1} J_2(2k_0 a \sin \theta) \right) \quad (15)$$

where  $J_i$  ( $i = 0, 1, 2$ ) represents the Bessel function of first kind of order  $i$ .

When  $\theta > \pi - \theta_{ca}$  and  $2k_0 a \sin \theta_{ca} = 2.44$ , the contribution from scatterers  $P_1$  and  $P_2$  can be expressed as [22]:

$$\sqrt{\sigma_1} e^{j\psi_1} + \sqrt{\sigma_2} e^{j\psi_2} = \sqrt{\pi} a \frac{J_1(2k_0 a \sin \theta)}{\sin \theta} e^{-j\frac{\pi}{2}}. \quad (16)$$

## ACKNOWLEDGMENT

This work was supported by The Major Research Plan of National Natural Science Foundation of China under Grant no. 61490690, 61490695.

## REFERENCES

- [1] V. C. Chen, F. Y. Li, S. S. Ho, and H. Wechsler, "Analysis of micro-doppler signatures," *IEEE IET Proc.-Radar Sonar Navig.*, vol. 150, no. 4, pp. 271-276, 2003.
- [2] V. C. Chen, F. Y. Li, S. S. Ho, and H. Wechsler, "Micro-Doppler effect in radar: Phenomenon, model, and simulation study," *Trans. Electron Syst.*, vol. 42, no. 1, pp. 2-21, 2006.
- [3] Y. Kim and T. Moon, "Human detection and activity classification based on micro-doppler signatures using deep convolutional neural networks," *IEEE Geoscience and Remote Sensing Letters*, vol. 13, no. 1, pp. 1-5, 2015.
- [4] H. W. Gao, L. G. Xie, S. L. Wen, and Y. Kuang, "Micro-doppler signature extraction from ballistic target with micro-motions," *IEEE Transactions on Aerospace and Electronic Systems*, vol. 46, no.4, pp. 1969-1982, 2010.
- [5] J. Lei, "Target classification based on micro-doppler signatures," *Proceedings of the IEEE International Radar Conference*, pp. 179-183, 2005.
- [6] Y. Yang and J. Lei, "Target classification and pattern recognition using micro-doppler radar signatures," *Proceedings of the Seventh ACIS International Conference on Software Engineering, Artificial Intelligence, Networking, and Parallel/Distributed Computing*, pp. 213-217, 2006.
- [7] J. Li and H. Ling, "Application of adaptive chirplet representation for ISAR feature extraction from targets with rotating parts," *IEE Proceedings of Radar Sonar and Navigation*, vol. 150, no. 4, pp. 284-291, 2003.
- [8] S. Ljubisa, D. Igor, and T. Thayanathan, "Separation of target rigid body and micro-doppler effects in ISAR imaging," *IEEE Transactions on Aerospace and Electronic Systems*, vol. 42, pp. 1496-1506, 2006.
- [9] A. Bultan, "A four-parameter atomic decomposition of chirplets," *IEEE Transactions on Signal Processing*, vol. 47, pp. 731-745, 1999.
- [10] K. Li, Y. Liu, and K. Huo, "Estimation of micro-motion parameters based on cyclostationary analysis," *IET Signal Processing*, vol. 4, no. 3, pp. 218-223, 2010.
- [11] Y. Liu, K. Li, and Z. Zhuang, "Estimation of micro-motion parameters based on micro-doppler," *IET Signal Processing*, vol. 4, no.3, pp. 213-217, 2010.

- [12] Y. LeCun, B. Boser, J. S. Denker, D. Henderson, R. E. Howard, W. Hubbard, and L. D. Jackel, "Handwritten digit recognition with a back-propagation network," *Advances in Neural Information Processing Systems*, vol. 2, no. 2, pp. 396-404, 1990.
- [13] A. Krizhevsky, I. Sutskever, and G. Hinton, "ImageNet classification with deep convolutional neural networks," *Adv. Neural Inf. Process. Syst.*, vol. 25, pp. 1090-1098, 2012.
- [14] C. Szegedy, W. Liu, Y. Jia, et al., "Going deeper with convolutions," *2015 IEEE Conference on Computer Vision and Pattern Recognition (CVPR) IEEE*, 2015.
- [15] G. Hinton, et al., "Deep neural networks for acoustic modeling in speech recognition," *IEEE Signal Process. Mag.*, vol. 29, no. 29, pp. 82-97, 2012.
- [16] T. Mikolov, A. Deoras, D. Povey, L. Burget, and J. Cernocky, "Strategies for training large scale neural network language models," *Automatic Speech Recognition & Understanding*, pp. 196-201, 2011.
- [17] R. M. Murray, Z. Li, and S. S. Sastry, *A Mathematical Introduction to Robotic Manipulation*. CRC Press, Boca Ration, 1994.
- [18] J. M. O'Toole and B. Boashash, "Fast and memory-efficient algorithms for computing quadratic time-frequency distributions," *Applied and Computational Harmonic Analysis*, vol. 35, no. 2, pp. 350-358, 2013.
- [19] L. C. Potter, D. M. Chiang, R. Carriere, and M. J. Gerry, "A gtd-based parametric model for radar scattering," *IEEE Transactions on Antennas and Propagation*, vol. 43, no. 10, pp. 1058-1067, 2002.
- [20] A. B. Gorji, B. Zakeri, and R. C. Janalizadeh, "Physical optics analysis for RCS computation of a relatively small complex structure," *The Applied Computational Electromagnetics Society Journal*, vol. 29, no. 7, pp. 530-540, 2014.
- [21] J. Perez and M. F. Catedra, "Application of physical optics to the RCS computation of bodies modeled with NURBS surfaces," *IEEE Transactions on Antennas and Propagation*, vol. 42, no. 10, pp. 1404-1411, 1994.
- [22] R. A. Ross, *Investigation of Scattering Principles. Vol III. Analytical Investigation General Dynamics*, Forth-worth, Texas, 1969.



**Gaogui Xu** received the B.S. degree and the M.S. degree in Computer Application Technology from China Three Gorges University, Hubei Province, China, in 2014 and 2017 respectively.

He is currently pursuing the Ph.D. degree of Electromagnetic Field and Microwave Technology at Communication University of China, Beijing, China. His research interests include micro-Doppler, micro-motion, target recognition, and deep learning.



**HongCheng Yin** was born in Yujiang, Jiangxi Province, China, in 1967. He received the B.S. degree in 1986 from Northwest Telecommunication Engineering Institute, Xi'an, China; the M.S. degree in 1989 from the Science and Technology on Electromagnetic Scattering Laboratory, and the Ph.D. degree in 1993 from Southeast University, Nanjing, China, all in electromagnetic field and microwave technique.

He is now a Research Scientist of Science and Technology on Electromagnetic Scattering Laboratory, Beijing, China. He has coauthored four books and published more than 130 papers in technical journals and conferences. His research interests include electromagnetic scattering, radar target signature, and radar target identification.

He is a fellow of Chinese Institute of Electronics.



**Chunzhu Dong** was born in 1981. He received the B.S. degree in Zhengzhou University, Henan Province, China, in 2004; the M.S. degree and the Ph.D. degree in Electromagnetic Field and Microwave Technology from the Communication University of China, Beijing, China, in 2007 and 2015 respectively.

Currently he is a Senior Engineer of Science and Technology on Electromagnetic Scattering Laboratory, Beijing, China. His research interests include radar target signature, electromagnetic scattering, and microwave technique.